Journal of Power Sources 195 (2010) 3969–3976

Contents lists available at ScienceDirect

Journal of Power Sources

journal homepage: www.elsevier.com/locate/jpowsour

Sol–gel processed thin-layer ruthenium oxide/carbon black supercapacitors: A revelation of the energy storage issues

V.V. Panić, A.B. Dekanski*, R.M. Stevanović

Institute of Chemistry, Technology and Metallurgy, Department of Electrochemistry, University of Belgrade, Njegoševa 12, Belgrade 125213, Serbia

ARTICLE INFO

Article history:
Received 11 September 2009
Received in revised form 9 December 2009
Accepted 3 January 2010
Available online 21 January 2010

Keywords:
Electrochemical supercapacitors
Oxide sols
RuO_2
RuO_2/C composite
Pseudocapacitance

ABSTRACT

Hydrous ruthenium oxide/carbon black nanocomposites were prepared by impregnation of the carbon blacks by differently aged inorganic RuO_2 sols, *i.e.* of different particle size. Commercial Black Pearls 2000® (BP) and Vulcan® XC-72 R (XC) carbon blacks were used. Capacitive properties of BP/RuO_2 and XC/RuO_2 composites were investigated by cyclic voltammetry (CV) and electrochemical impedance spectroscopy (EIS) in H_2SO_4 solution. Capacitance values and capacitance distribution through the composite porous layer were found different if high- (BP) and low- (XC) surface-area carbons are used as supports. The aging time (particle size) of Ru oxide sol as well as the concentration of the oxide solid phase in the impregnating medium influenced the capacitive performance of prepared composites. While the capacitance of BP-supported oxide decreases with the aging time, the capacitive ability of XC-supported oxide is promoted with increasing oxide particle size. The increase in concentration of the oxide solid phase in the impregnating medium caused an improvement of charging/discharging characteristics due to pronounced pseudocapacitance contribution of the increasing amount of inserted oxide. The effects of these variables in the impregnation process on the energy storage capabilities of prepared nanocomposites are envisaged as a result of intrinsic way of population of the pores of carbon material by hydrous Ru oxide particle.

© 2010 Elsevier B.V. All rights reserved.

1. Introduction

In contrast to classic parallel-plate capacitors, which store energy through induced electric field in dielectric medium of mm thickness, the capacitance of electrochemical capacitors (EC) originates from characteristic physico-chemical properties of a double layer (of nm thickness) which generates in the electrode/electrolyte interphase. The strength of electric field can reach even 10^9 V m^{-1}, thus bridging the energy/power gap between parallel-plate capacitors and batteries as EC super-, or even ultra-capacitors [1]. Besides electrostatic energy storage through double layer charging/discharging, basically associated to high-surface-area carbon materials [2,3], some noble metal oxides, such as RuO_2 [4–12], IrO_2 [13–14] and Co_3O_4 [15–17], and conductive polymers can store energy chemically by reversible redox transitions, causing their pseudocapacitive behaviour [1].

One of the most investigated pseudocapacitive materials is ruthenium oxide, which exhibits excellent capacitive performance due to several metal-ion redox transitions, close in energy, *i.e.* spread over wide potential range [6]. In fabrication of supercapacitive material, the oxide is usually supported in the composites by other materials of extended surface area, which are of high double layer capacitance and able to distribute finely the oxide nanoparticles over its surface, such as carbon blacks, fibbers or tubes [18–28].

Although the capacitance of the carbon support can be considerably increased due to pseudocapacitive contribution of inserted ruthenium oxide, the real surface area of the composite is smaller in comparison to carbon support [21,27,29]. This is since oxide particles can block the internal surface of carbon support, and consequently the capacitive efficiency of the composite can be suppressed. Pico et al. [25] investigated the capacitive performance of carbon/RuO_2 composites prepared from meso- and micro-porous carbon impregnated by the oxides of two different particle sizes. Due to blocking issue, they found meso-porous carbon combined with smaller oxide particles as more suitable for capacitance application than micro-porous one. In the case of carbon fibre capacitive material, Lee et al. [30] found that the capacitance distribution throughout the capacitive layer is mainly governed by pore length distribution, rather than by pore size distribution. In addition, there is an electrolyte accessibility issue to the internal surface of high-surface-area carbon blacks, which lowers their energy storage ability in fast charging/discharging processes [31,32].

Bearing in mind above considerations, it appears a strong motif to investigate what could be the right choice of carbon black if it should be combined in composites with the oxide of controllable morphology. It was shown [33,34] that forced hydrolysis of metal

* Corresponding author. Tel.: +381 64 3640 231; fax: +381 11 3640 234.
E-mail address: dekanski@ihtm.bg.ac.rs (A.B. Dekanski).

0378-7753/$ – see front matter © 2010 Elsevier B.V. All rights reserved.
doi:10.1016/j.jpowsour.2010.01.028

chlorides in acid medium produces the oxide dispersions with particle size which can be easily controlled by the duration of forced hydrolysis process itself, *i.e.* by the aging of oxide sols. In continuation to the previously published paper [31], in which capacitive performance of two carbon black materials of considerably different surface area, Black Pearls 2000® (BP) and Vulcan® XC-72 R (XC), was analyzed in detail from the standpoint of electrolyte and input signal accessibility to the internal surface, the aim of the present work is to analyze the energy storage properties of BP/and XC/RuO_2 composites. The blocking and accessibility issues are investigated by impregnating the sol–gel processed oxide from the previously prepared sols (forced hydrolysis process) of different aging time (particle size) and by changing the amount of oxide impregnated through the control of the concentration of oxide solid phase in the impregnating medium. The structure of the composite and an in-depth capacitance distribution throughout composite layer is proposed according to the results of electrochemical impedance spectroscopy investigations.

2. Experimental

Composites were obtained by impregnation of the carbon blacks with hydrous ruthenium oxide, from previously prepared suspensions of carbon blacks and RuO_2 sols of different aging times (2.5, 8, 24 and 46 h).

Colloidal dispersion of ruthenium oxide was prepared by forced hydrolysis of 5.0 g $RuCl_3$ ($RuCl_3{\cdot}xH_2O$ dried at 120 °C for 24 h in nitrogen atmosphere) in 0.27 mol dm^{-3} HCl at boiling temperature [19] which should give the concentration of the solid phase of about 0.65 mass% in the resulting oxide sol, calculated to RuO_2. The starting solution was aged for 2.5, 8, 24 and 46 h (aging time, the duration of the forced hydrolysis process). The final concentration of the solid phase for all ageing times was found to be around 1.0 mass% (dry residue treated in air at 120 °C for 24 h), which indicates the presence of highly hydrated oxide [19].

The impregnation process was conducted in prepared suspensions by ultrasonication for 30 min, followed by centrifugal solid phase separation from the impregnating medium. In order to examine influence of oxide phase concentration in the impregnating medium, c_{IM} (and consequently the oxide content in the composite), on the composite properties, volume ratio of carbon BP suspension and oxide sol aged for 24 h were mixed in different volume ratios. In that way, impregnating mediums with oxide phase contents of 2.2, 5.5 and 8.8 g dm^{-3} were obtained. In the further text, composites will be denoted by general labels: C/Rt_a, where C stands for carbon substrate type (BP or XC), R for RuO_2, t_a for aging time of RuO_2 sol (where for the sake of conciseness tag 2 was used for t_a = 2.5 h).

Prepared composites were dried at 110 °C for 24 h. The oxide content in composites obtained by impregnation of carbon BP was between 20 and 40 mass%, depending on t_a and c_{IM}.

The surface appearance of some of prepared composites was checked by scanning electron microscopy, using a JEOL microscope, model JSM-T20 (U_w = 20 kV).

Formation of the composite thin-layer at Au and glassy carbon rotating disk electrodes was done in the same manner as in the earlier investigation on capacitive properties of carbon blacks [31]. Aqueous suspension, with concentration of the solid phase of 3.0 g dm^{-3}, was preconditioned in an ultrasonic bath for 1 h. Applied amount of the suspension corresponded to deposited composite layer mass of 0.233 cm^{-2}. After application of the aqueous suspension, composite layer was dried at the room temperature, and subsequently Nafion® aqueous solution was applied on top of the layer. Finally, the electrode assembly was dried again at room temperature for 12 h. By applying thin electrode layers, the intergranular conductivity issues as well as the transition from resistive to capacitive behaviour, as reported in literature for thick layers [35–37], are shifted to higher frequencies in impedance spectra. Hence, the investigation of capacitance distribution within prepared composite layers at open circuit potential, which is mostly reflected in low-frequency domain, can be extended to wider frequency range and be freed of mentioned conductivity issues which are out of the scope of this paper.

Cyclic voltammetry (CV) measurements were performed in deaerated 0.50 mol dm^{-3} H_2SO_4, at room temperature (23 ± 1 °C), with saturated calomel electrode (SCE) as a reference and platinum mash as a counter electrode. Experiments were conducted using potentiostats AG&G PAR, model 273A and BAS, model CV-27.

Electrochemical impedance spectroscopy (EIS) experiments were carried out at the potential of 0.55 V (close to open circuit reading), in deaearated 0.50 mol dm^{-3} H_2SO_4. Measurements were performed by employing potentiostat/galvanostat AG&G PAR 273A, connected to AG&G PAR 5301 *lock-in* amplifier, or in some cases by employing femtostat model FAS32, GAMRY Instruments (Warminster, PA). Working electrode response was recorded for the sinusoidal input signal of ±10 mV (root mean square). Appropriate PC computer software was employed for data acquisition. The EIS data analysis was done by ZView® software, version 2.6, Scribner Associates Inc. (Southern Pines, NC).

3. Results and discussion

3.1. Capacitive characteristics of BP/R composites

Cyclic voltammograms of BP/R composites, obtained from differently aged oxide sol and the lowest oxide concentration in the impregnating medium (2.2 g dm^{-3}) are shown and compared to BP response in Fig. 1. Cyclic voltammograms are of similar, roughly rectangular shape indicating capacitive behaviour of the composite in this potential range. It is seen that aging time considerably affects intensity of voltammetric currents. For shorter aging times, voltammetric currents are similar to that of BP (t_a = 2.5 h) or somewhat higher (t_a = 8 h) than those obtained for BP. However, for longer aging times (24 and 46 h) voltammetric currents for the composites are lower than those for BP. Since mass gain was found for all samples upon impregnation, inferior characteristics registered at applied cyclic charging/discharging could not be related to the lack of impregnation. The causes for such, at first glance, paradoxical capacitive properties of BP/R 24 and BP/R 46 composites could be

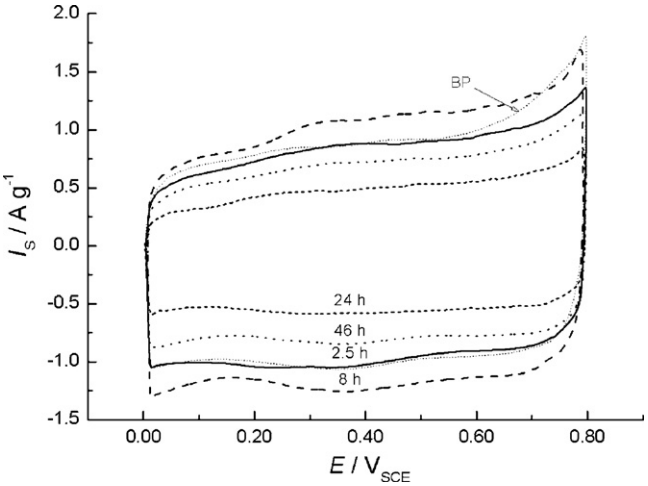

Fig. 1. Cyclic voltammograms of BP/R composites, obtained from RuO_x sol of different aging time, c_{IM} = 2.2 g dm^{-3}; ν = 10 mV s^{-1}.

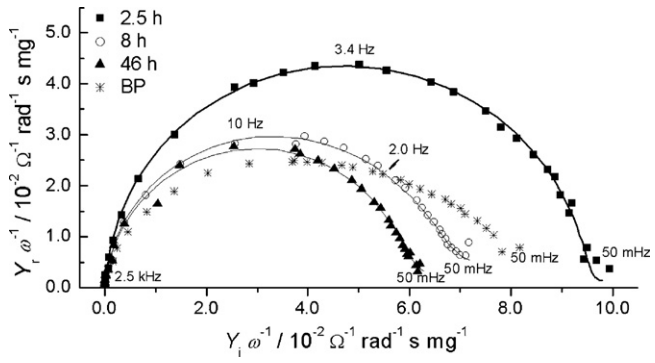

Fig. 2. Capacitance complex plane plots of BP and BP/R composites obtained from RuO_x sols of different aging time (c_{IM} = 2.2 g dm^{-3}); potential: 0.55 V. The EIS data of equivalent electrical circuits are given by lines (for the fitting of BP EIS data see [31]).

caused by intrinsic relationship between particle size distribution, which changes with the aging time, and the morphology of the impregnated carbon black support. Generally, registered voltammetric currents decrease with aging time with some exceptions discussed later, *i.e.* with particle growth during the aging of the sol [33].

More detailed insight into capacitive properties of obtained composites, *i.e.* capacitance distribution through the composite layer, could be obtained from the analysis of their impedance characteristics at the potential close to that of open circuit reading. In Fig. 2, capacitance complex plane plots of BP, BP/R 2, BP/R 8 and BP/R 46 are given together with plot for carbon substrate [31]. BP/R 24 composite was not considered due to its worst characteristics. The plots consist of capacitive loops of decreasing radius with aging time of the sol, *i.e.* composite capacitance decreases with aging due to the increase in oxide particle size.

Although the capacitance plot of BP consists of at least two overlapped capacitive loops, only one loop can be clearly seen for composites. The lowest admittance values (both the imaginary and real part) were registered for BP at the frequencies down to 2.0 Hz. This indicates that a part of composite surface which is easily accessible to the electrolyte is of larger capacitive ability than corresponding part of BP surface, due to presence oxide particles. However, at the frequencies below 2.0 Hz the admittance of BP becomes much larger than that of BP/R 8 and BP/R 46 composite, due to appearance of an additional capacitive loop.

With an exception of BP/R 8 composite that is discussed latter on, results are in accordance with those obtained by cyclic voltammetry (Fig. 1).

Impregnation of carbon black by hydrated ruthenium oxide always causes decrease in BET real surface [21,38–40]. This decrease in real surface becomes more pronounced with an increase in oxide mass fraction [38,41]. However, the decrease in real surface area is accompanied with an increase in composite capacitance caused by oxide pseudocapacitance, which apparently prevails over the reduction in carbon double layer capacitance due to the decrease in real surface area. These effects of impregnation are more pronounced if real surface area of carbon substrate is larger. However, if oxide fraction in composite is rather small, and if oxide particles are enough large, pseudocapacitive contribution of the oxide is not sufficient to prevail, or at least to compensate, the decrease in double layer capacitance caused by decrease in real surface area of carbon substrate. Hence, at certain impregnation conditions (leading to small oxide fraction and/or large oxide particles) and at rather high charging/discharging rates, capacitive properties of the composite may manifest as even worse with respect to the capacitive properties of carbon substrate.

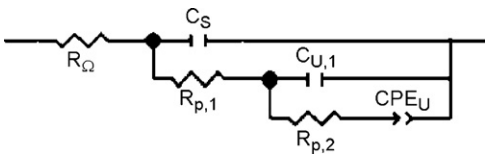

Fig. 3. Equivalent electrical circuit used to simulate EIS data of BP/R composites.

Equivalent electrical circuit used to fit the impedance data from Fig. 2 is shown in Fig. 3. The circuit of transmission line type, with three transmission branches, was required to describe satisfactory the impedance characteristics of composites (Chi-squared based on modulus calculated was below 0.001, while relative error of the parameter values of the elements did not exceed 20%). The assignment of circuit elements is the same as already described in analysis of EIS behaviour of carbon substrate [31]. In that study [31], transmission line circuit with five branches was required to be employed for the impedance characteristics of the carbon substrate, pointing the more complex capacitance distribution through the BP layer with respect to composite layer. However, a five-branch circuit gave also good fitting results for the composite with smallest oxide particles (2.5 h), which will be used to compare capacitance characteristics of this composite to carbon substrate in the section "Influence of the concentration of oxide phase in impregnating medium on the capacitive properties of BP/R composites".

Since qualitative difference between composite and carbon substrate is in the presence of the oxide phase, one should expect more complex morphology for composite layer. From the standpoint of EIS capacitive characteristics presented in this paper (Figs. 2 and 3) it is not the case. Specific capacitances and pore resistances, obtained by fitting the BP/R composite impedance data to the circuit from Fig. 3, are presented in Fig. 4 as the distribution throughout the illustrated porous composite layer.

Outer capacitance of composites (related to the surface of the layer which is directly exposed to the electrolyte bulk), C_S, given as first value of capacitance in electrolyte → substrate direction in Fig. 4, is for two orders of magnitude larger than outer capacitance of carbon substrate (0.32 F g^{-1} [31]), and decreases with aging time of the sol. Much larger outer capacitance composite in contrast to carbon substrate is a consequence of presence of oxide particles impregnated into the outer surface of carbon grains, represented by the sum of pseudocapacitance and double layer capacitance at electrolyte/oxide interface. Oxide particles grow with sol aging time of oxide sol, which causes the decrease in outer capacitances in series BP/R 2 > BP/R 8 > BP/R 46.

There is also a decrease in the values of inner capacitances (second value in electrolyte → substrate direction, $C_{U,1}$) with aging of the sol. However, the value obtained for BP/R 2 is comparable with the sum of inner capacitances of the carbon substrate from second to fourth branch (about 45 F g^{-1} [31]), while the inner capacitance of the BP/R 8 and BP/R 46 composites are lower with respect to BP, which is similar to the cyclic voltammetry results (Fig. 1).

However, the difference between capacitive behaviour of BP/R 8 composite, with respect to BP/R 2, as registered by cyclic voltammetry and EIS (Figs. 1 and 2, respectively), deserves additional attention. While CV measurements show beneficial capacitive performances of BP/R 8, EIS measurements (Figs. 2 and 4) indicate that capacitance of the composite obtained with the oxide of smaller particle size (BP/R 2) should be higher. In addition, the oxide particle size at the aging time of 8 h appears to be a "breaking point" for the change of the composite pore resistance distribution to considerably higher values (the values are lower for BP/R 2 composite than that of other composites). These findings indicate that small oxide particles of BP/R 2 composite are distributed over the surface of carbon grains, with the composite morphology resembling that

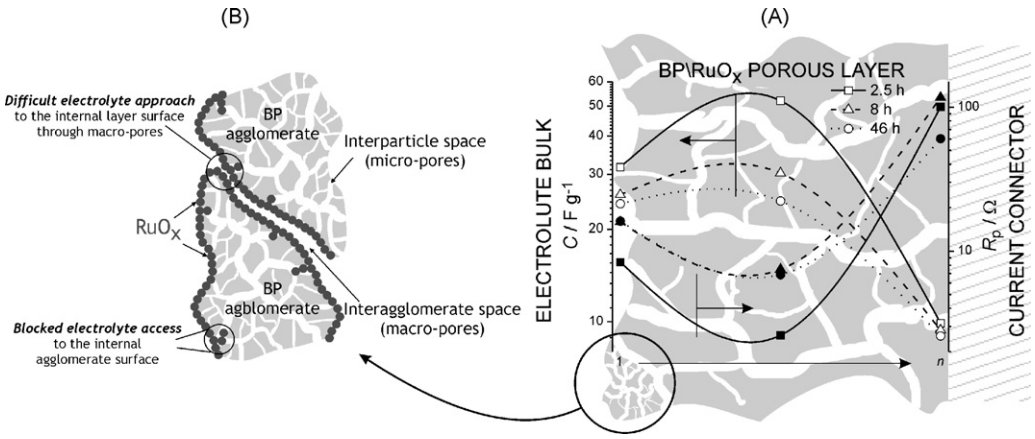

Fig. 4. Capacitance and pore resistance distribution throughout the porous layer of BP/R composite obtained from RuO_x sol of different aging time and the sketch of proposed oxide particles packing onto the surface of carbon substrate.

of carbon support and hindering the electrolyte access to the bare carbon surface. On the other hand, larger oxide particles tend to form a physical mixture with the carbon grains, causing the partial sealing of the pores between the carbon grains, and leaving considerable part of the surface of carbon grains uncovered. As the consequence, the anodic excursion of the potential above 0.70 mV in CV (Fig. 1) causes the formation of functional groups at the surface of carbon support in the case of BP/R 8 composite, which give additional contribution to the pseudocapacitance of this composite. It is seen that CV currents of BP/R 8 composite and carbon support in this potential region are quite similar, although they differ outside this potential region. The increase in capacitive ability of carbon/RuO_2 composite upon activation of carbon supports was also registered by Hu and Wang [28]. Such an increase in CV currents was not registered for BP/R 2 composite, which indicates that the oxide of smaller particles covers much tightly the surface of carbon support. Since in EIS measurements there is no such excursion to the potentials where the activation by the formation of functional groups on the surface of carbon support can take part, these measurements reflects only the hindering of the internal part of the surface of carbon grains in the case of BP/R 8 composite. Consequently, the EIS capacitive ability of BP/R 8 composite is smaller in comparison to BP/R 2 composite, which is opposite to CV findings. In addition, it should be expected that CV at a single sweep rate of 10 mV s^{-1} should reflect in a lesser degree the hindering of the internal surface of carbon grains than the EIS registered with sweeped frequency.

Decrease in composite inner capacitances with sol aging time is accompanied by the increase in pore resistance, $R_{p,1}$. Resistance in pores of BP/R 2 composites corresponds to resistances $R_{p,1}$ and $R_{p,2}$ of carbon substrate, while resistances in pores of BP/R 8 and BP/R 46 composites are larger than those for carbon substrate. This is a consequence of volume shrink of micropores (interparticle space within carbon grains) in which oxide particles gathered, thus hindering the approach of the electrolyte to the interior of carbon grains (Fig. 4). Oxide particles in BP/R 2 composite are smaller, being not able to cause considerable volume shrinkage of micropores within carbon grains. Accordingly, the value of inner capacitance for this composite is largest, since the contribution of oxide particles, situated in the carbon interparticle space, to overall composite capacitive characteristics is more pronounced.

Inner capacitance of the composite represented by constant phase element in the third branch of equivalent circuit in Fig. 3 (third value in the electrolyte → substrate direction at Fig. 4), is much lower than inner capacitance of the second branch and does not depend considerably on the aging time. This capacitance value is for an order of magnitude lower than corresponding value for carbon substrate (about 10 and 150 F g^{-1} [31], respectively). However, the associated pore resistance, $R_{p,2}$, is similar to the corresponding value of $R_{p,3}$ for carbon substrate, which implicates that inner capacitance in the third circuit branch is associated to morphologically similar parts of porous composite layer and carbon substrate—to those corresponding to internal surface of the carbon grains. For these parts of the surface, impregnation failed, since large oxide particles on the top had closed the pore orifices at the surface of carbon grains. These oxide particles at the surface of carbon grains block the electrolyte access to porous interior of carbon grains, thus leaving it even dry and making it capacitively inactive. This should cause the values of inner capacitance of the composites from the third branch to be much smaller than that of carbon substrate.

These considerations are illustrated by a sketch given in Fig. 4.

3.2. Influence of the concentration of oxide phase in impregnating medium on the capacitive properties of BP/R composites

An increase in the oxide phase concentration in the impregnating medium, c_{IM}, leads to an improvement of the capacitive properties of the composite. Since only BP/R 2 composite capacitive characteristics can be analyzed by the same equivalent circuit as that of BP, this composite was chosen for the detailed investigation of the influence of the concentration of oxide phase in impregnating medium on the composite capacitive behaviour. Cyclic voltammograms of BP/R 2 composite obtained with different c_{IM} are shown in Fig. 5. The increase in c_{IM} from 2.2 to 5.5 g dm^{-3} is followed by the increase in voltammetric currents, while additional increase in concentration to 8.8 g dm^{-3} does not produce significant increase in the currents. Cyclic voltammograms from Fig. 5 indicate that maximum efficiency of impregnation is achieved with concentration of 5.5 g dm^{-3}; additional increase in concentration does not result in an improvement of the capacitive characteristics of the composite.

Anodic voltammetric currents at 0.55 V for composites obtained with concentrations of 5.5 and 8.8 g dm^{-3} are quite similar and noticeably higher than for the composite obtained at the concentration of 2.2 g dm^{-3}. However, EIS results and simulation by equivalent electric circuit at 0.55 V suggest different capacitive characteristics of composites obtained with different concentrations of oxide phase in the impregnating medium. Admittance complex plane plots, obtained at the potential of 0.55 V, for composites obtained at different concentrations of the oxide phase in the impregnating medium are shown in Fig. 6. For the composite obtained with concentration of 8.8 g dm^{-3} the admittance is lower than for composite obtained with concentration of 5.5 g^{-3}. Admittance data for composite obtained with concentration of 8.8 g dm^{-3}

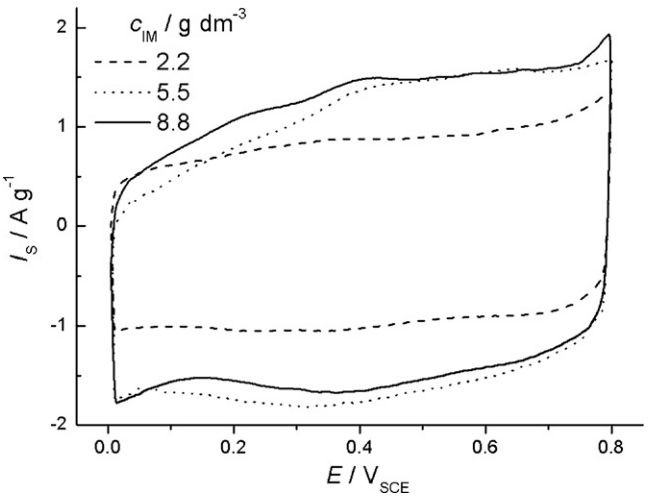

Fig. 5. Cyclic voltammograms of BP/R 2 composite obtained from impregnating media with different concentration of oxide phase, c_{IM}. Sweep rate: 10 mV s^{-1}.

appear as at least two highly overlapped capacitive loops (4.8 Hz to 15 kHz and 50 mHz to 1.6 Hz).

Five-branch equivalent electrical circuit [31] was employed for fitting the impedance data from Fig. 6, and the fitting results are shown in Fig. 6 by solid lines. The values of the equivalent electrical circuit parameters are shown in Fig. 7 as capacitance and resistance distribution throughout composite porous layer for different c_{IM}. The plane $c_{IM} = 0$ contains previously reported data [31] of carbon substrate.

Outer, and partially the inner coating capacitances (up to the forth value in the $1 \rightarrow n$ direction in Fig. 7a), are increased considerably with respect to BP (plane $c_{IM} = 0$) when the concentration increases up to 5.5 g dm^{-3}. To this increase in capacitive ability corresponds a decrease in pore resistances (first and second value in the $1 \rightarrow n$ direction in Fig. 7b), which means that corresponding parts of the 3D layer surface became more easily accessible to the electrolyte with the increase in c_{IM}. This is the consequence of an increasing amount of the oxide at the surface of carbon grains.

The inner capacitance, given as fifth value in the $1 \rightarrow n$ direction in Fig. 7a (derived from CPE_U parameters), is subjected to a fourfold increase when c_{IM} increases from 2.2 to 5.5 g dm^{-3}, but the value is still lower than that of BP. Bearing in mind that inner surface of the carbon grains is already blocked at 2.2 g dm^{-3} (the sketch from Fig. 4), it can be supposed that this capacitance is subjected to "assignment transition" from inner surface of BP grains to the inner surface of an oxide layer laying at the surface of BP grains, which thickness increases with c_{IM}. This consideration is particularly supported by further increase in fifth value of the capacitance when c_{IM} is additionally increased to 8.8 g dm^{-3}. At this concentration, the fifth value of the capacitance for the composite is even higher than corresponding value for BP, while all the values of pore resistance at this concentration are higher than for the composite obtained at c_{IM} of 5.5 g dm^{-3} as the consequence of increased thickness of the oxide layer that wraps carbon grains.

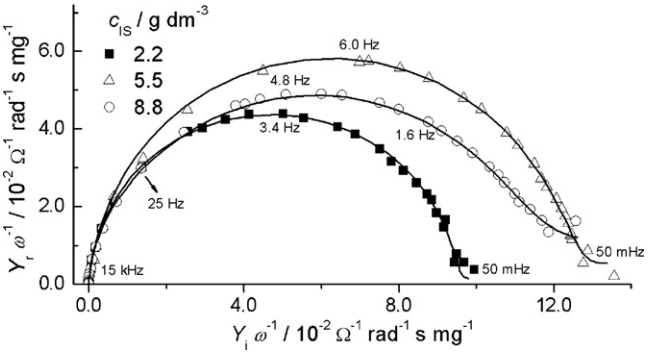

Fig. 6. Admittance complex plane plots of BP/R 2 composite obtained from impregnating media with different concentration of oxide phase, c_{IM}. EIS data of equivalent electrical circuit are given by lines.

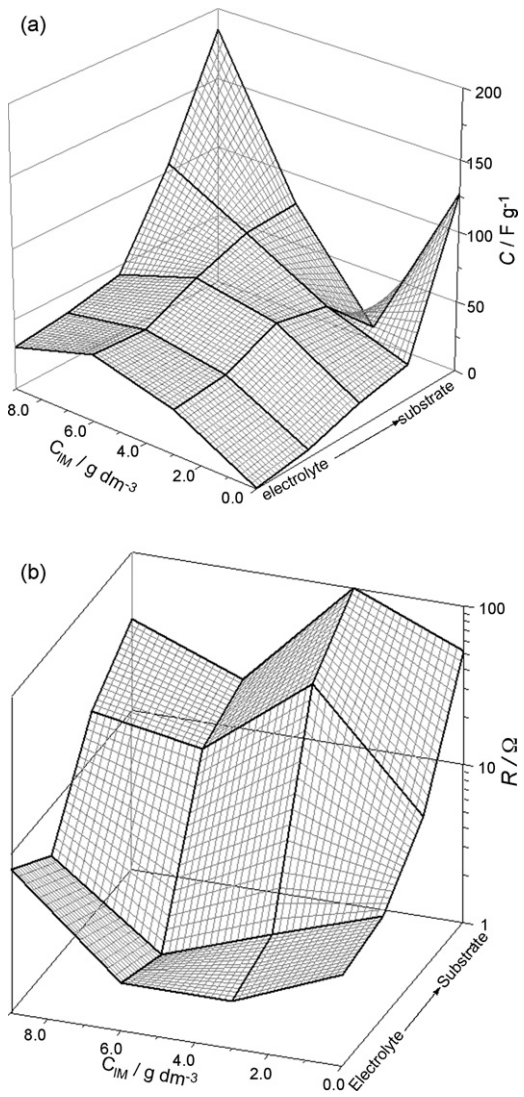

Fig. 7. Capacitance (a) and pore resistance (b) distribution throughout the porous layer of BP/R 2 as the function of oxide phase concentration in the impregnating medium, c_{IM}. Data for carbon substrate are given for $c_{IM} = 0$.

It follows from above considerations that combination of high-surface-area BP carbon black and small oxide particles can hardly lead to superior capacitive performance of BP/RuO_2 composite. Since oxide particles block the pore orifices of the carbon grains, the interior, *i.e.* most of the extended carbon surface area, is inaccessible, and BP support (in a "grained" form) acts only as a pattern for impregnation and carrier of capacitively active oxide. In the following Section, the capacitive characteristics of a low-surface-area XC carbon black/RuO_2 composite, prepared by impregnation with differently aged RuO_2 sols are given.

3.3. Capacitive characteristics of XC/R composite

Since optimal concentration of the oxide solid phase for impregnation of BP was found to be 5.5 g dm^{-3}, this concentration was

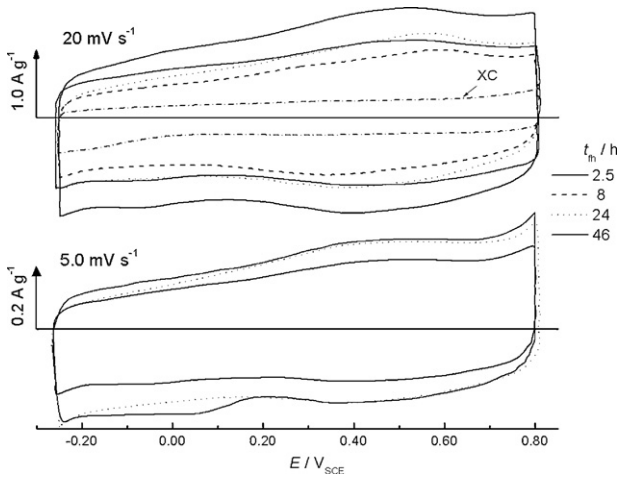

Fig. 8. Cyclic voltammograms at different scan rates of XC/R composite obtained from RuO_x sol of different aging time, $c_{IM} = 5.5\ g\ dm^{-3}$.

chosen for impregnation of XC and examination of oxide sol aging effects on capacitive characteristics of the composite. It is to be noted that due to low wetability of XC, composite capacitive characteristics were found dependent on the time passed from the moment of immersion into the electrolyte [42]. Hence, all of the results presented in this section were collected at fixed time upon immersion. Cyclic voltammograms of the XC/R composites, registered at two different scan rates, are shown in Fig. 8.

Voltammetric currents for XC/R composites are much larger than those obtained for carbon XC substrate. Current peaks at about 0.45 V correspond to ruthenium oxide pseudocapacitive redox transition. Couple of less pronounced current peaks at potential of −0.05 V originate from reduction of carbon surface oxygen groups, which were formed upon anodic activation of carbon. Changes in position and intensity of current peaks reveal that upon decrease in potential sweep rate contribution of carbon substrate to the overall voltammetric response becomes more pronounced, as it is reported earlier [31].

Capacitance complex plane plots of XC/R composites obtained using oxide sols of different aging times are shown in Fig. 9. The diagram for XC/R 2 differs in shape from those obtained for other two composites, and appears similar to the diagram of carbon substrate [31]. For XC/R 2 composite, high-frequency capacitive loop is followed by a tail-shaped low-frequency loop, which appeared at lower frequencies than corresponding loops of carbon substrate [31]. In addition, the increase in imaginary part at low frequencies,

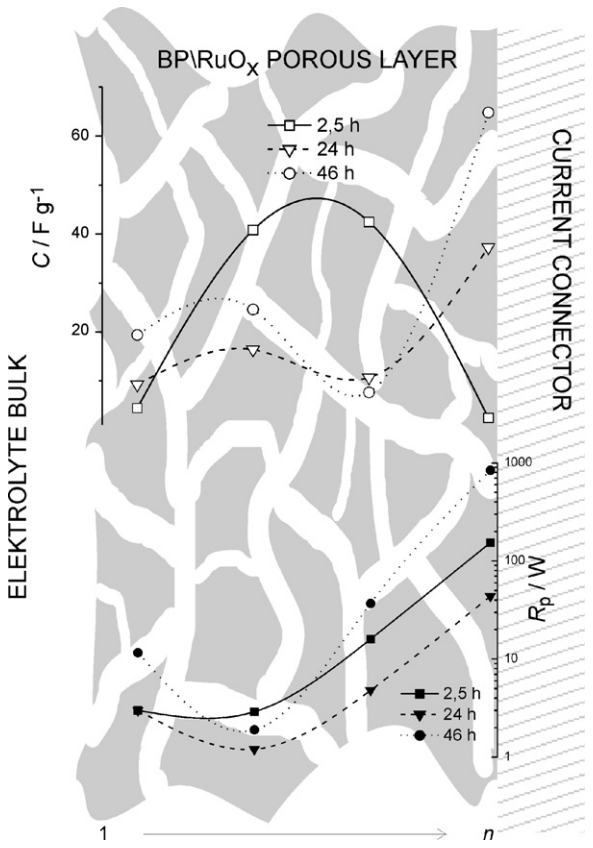

Fig. 10. Capacitance and pore resistance distribution throughout the porous layer of XC/R composite obtained for the sols of different aging times.

seen for XC [31], is not registered for XC/R 2 composite. In previous study [31], this increase was assigned to charge transfer resistance related to quinone/hydroquinone redox transition. This resistance does not emerge in EIS data for composites since carbon surface is sheltered by the oxide.

Fitting of the impedance data of XC/R composites were also performed to equivalent electrical circuit of transmission line type. The circuit consisted of four branches, one more with respect to XC [31] and without charge transfer resistance in parallel, which was required for XC. The elements arrangement in the circuit for XC/R 2 composite differed from those in the circuit for other two composites (inset of Fig. 9). For XC/R 2 composite, capacitance of inner surface is represented by constant phase elements in first three

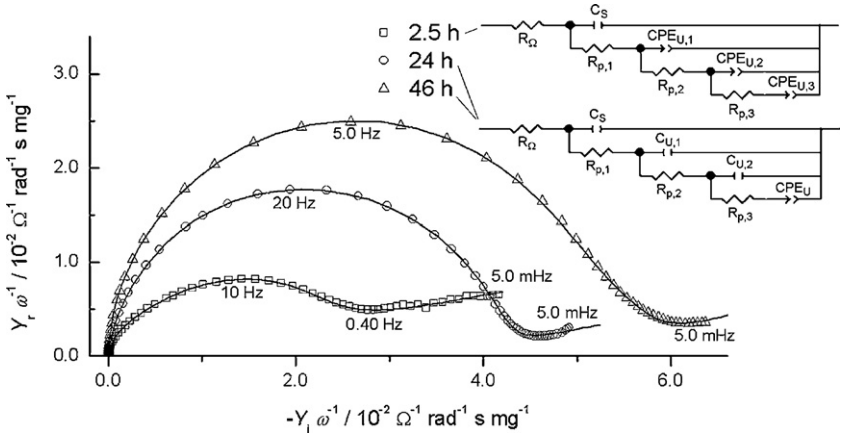

Fig. 9. Capacitance complex plane plots of XC/R composite obtained from the sols of indicated aging times ($c_{IM} = 5.5\ g\ dm^{-3}$). Electrolyte: 0.50 mol dm^{-3} H_2SO_4; potential: 0.55 V. Inset: equivalent electrical circuits used to fit the data.

branches, while for other composites CPE is used only in the last, fourth, branch of the circuit. This could mean that the morphology of XC/R 2 composite is much like that of XC carbon substrate, since its inner capacitances were also represented by constant phase elements [31].

Impedance characteristics of equivalent electric circuits are represented by lines in Fig. 9, while the values of parameters are given in Fig. 10 as capacitance and resistance distribution across illustrated porous layer of the XC/R composite. Outer composite capacitance, C_S, increases with aging time, opposite to the case of BP/R composites (Fig. 4). Although outer capacitance of the composites obtained with BP is considerably larger than that of BP, outer capacitance of XC/R 2 composite (about 4 F g^{-1}, Fig. 10) is only doubled in comparison to XC substrate (1.8 F g^{-1} [31]). However, outer capacitance of XC/R 46 composite (about 20 F g^{-1}) is for an order of magnitude larger than outer capacitance of the XC. This, as well as equivalent circuit arrangement (Fig. 9) and SEM results for XC substrate [31], XC/R 2 and XC/R 46 composites – those of composites are shown in Fig. 11 – clearly points out that the impregnation of carbon outer surface is weak in the case of XC/R 2 composite, while it becomes pronounced only with XC/R 46 composite. The surface appearance of XC/R 2 composite (Fig. 11a) is quite similar to the loose structure of XC layer ([31] and Fig. 3c therein), while more compact structure of the grains pasted together is seen in surface appearance of XC/R 46 composite (Fig. 11b).

Inner capacitances of the XC/R 2 composite porous layer (second and third value in the equivalent circuit in the $1 \rightarrow n$ direction in Fig. 10) is much larger than outer, while in the cases of XC/R 24 and XC/R 46 composite these two capacitances are similar. Associated pore resistances increase, while lowest resistance is obtained for XC/R 24 composite. However, the values of these pore resistances obtained for the XC/R composite layers are considerably lower than corresponding value obtained for XC (about 120 Ω [31]), but quite similar to the values obtained for BP/R composites, which is also the case with the values of inner capacitances (Fig. 4). This suggests that these circuit parameters are to be assigned rather to the oxide than to the carbon substrate. Second and third value of the inner capacitance of XC/R 2 composite is much larger than corresponding capacitances of XC/R 2 and XC/R 46 composites. Therefore, largest capacitance at slow charging/discharging processes is going to be expected for XC/R 2 composite. This is seen as larger voltammetric currents registered for XC/R 2 composite in comparison to XC/R 46 composite at low sweep rate, while capacitive performances of the later are better at high sweep rate (Fig. 8), due to the larger outer capacitance (Fig. 10).

Fourth value of the inner capacitance of the XC/R 2 composite in the $1 \rightarrow n$ direction in Fig. 10, is significantly smaller than the second and third value of inner capacitance (Fig. 10). Taking into account corresponding resistance in the pores of about 170 Ω, this part of the inner capacitance should be considered to correspond to the capacitive response of hardly accessible parts of the inner oxide surface, located in the intergranular spaces of the carbon substrate. Similarly to the case of the BP/R 2 composite, reversibly formatted gel oxide phase hinders the electrolyte access to the composite inner surface.

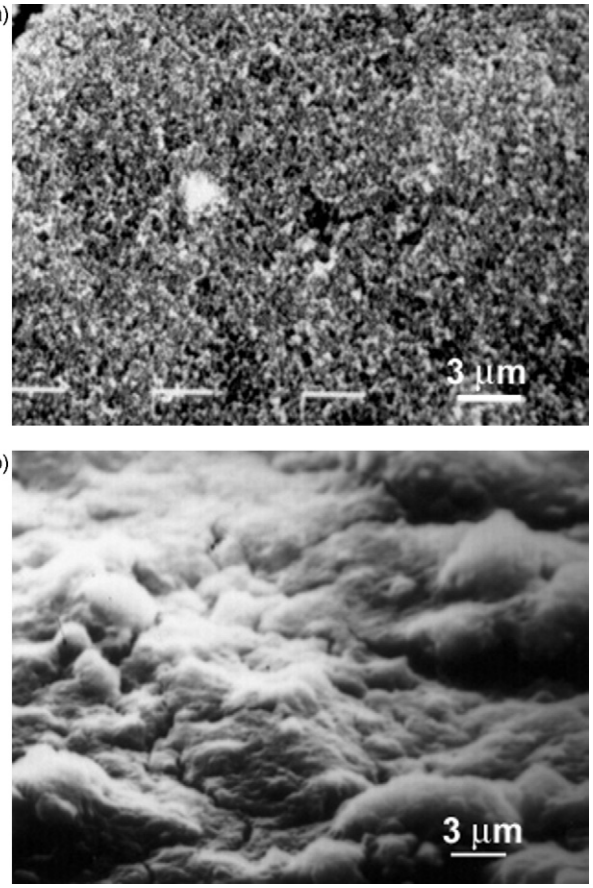

Fig. 11. SEM microphotographs of the surface of (a) XC/R 2 and (b) XC/R 46 composite.

4. Conclusion

The carbon black/RuO_2 composites prepared by sol–gel procedure from differently aged oxide sol and high-surface-area carbon (BP) have larger capacitance values than the composites prepared from low-surface area carbon (XC). Capacitance of the BP-supported composites decreases with aging of the oxide sol due to growth of the oxide particles, while the capacitance of XC-supported composites increases with the aging due to the low impregnation efficiency of small oxide particles. Increasing concentration of the oxide phase in the impregnating medium leads to the increase in capacitance of the BP/R composites. However, inner surface of the BP carbon substrate upon composite formation becomes hardly accessible to the electrolyte and rather inactive, as a result of pore blocking by the oxide particles at the top of the carbon grains. The best energy storage performances at low charging/discharging rates is going to be expected for the composites prepared from small oxide particles and low-surface-area carbon blacks, while the composites with high-surface-area carbon supports should suffer from the loss of energy storage ability of carbon double layer capacitor part.

Acknowledgement

This work was financially supported by the Ministry of Science and Technological Development of the Republic of Serbia, Contract No. B142048.

References

[1] B. Conway, Electrochemical Supercapacitors—Scientific Fundamentals and Technological Applications, Plenum Publishers, New York, 1999.
[2] E. Frackowiak, F. Béguin, Carbon 39 (2001) 937–950.
[3] F. Raimondi, G.G. Scherer, R. Kötz, A. Wokaun, Angew. Chem. Int. Ed. 44 (2005) 2190–2209.
[4] P. Kurzweil, J. Power Sources 190 (2009) 189–200.
[5] J.P. Zheng, P.J. Cygan, T.R. Jow, J. Electrochem. Soc. 142 (1995) 2699–2703.
[6] S. Ardizzone, S. Trasatti, Adv. Colloid Interface Sci. 64 (1996) 173–251.
[7] J.P. Zheng, Y. Xin, J. Power Sources 110 (2002) 86–90.
[8] W. Sugimoto, T. Kizaki, K. Yokoshima, Y. Murakami, Y. Takasu, Electrochim. Acta 49 (2004) 313–320.
[9] K.-M. Lin, K.-H. Chang, C.-C. Hu, Y.-Y. Li, Electrochim. Acta 54 (2009) 4574–4581.

[10] K. Kuratani, T. Kiyobayashi, N. Kuriyama, J. Power Sources 189 (2009) 1284–1291.
[11] Y.-Y. Liang, H.L. Li, X.-G. Zhang, J. Power Sources 173 (2007) 599–605.
[12] K. Kuratani, H. Tanaka, T. Takeuchi, N. Takeichi, T. Kiyobayashi, N. Kuriyama, J. Power Sources 191 (2009) 684–687.
[13] D.-Q. Liu, S.-H. Yu, S.-W. Son, S.-K. Joo, ECS Trans. 16 (2008) 103–109.
[14] A.A.F. Grupioni, E. Arashiro, T.A.F. Lassali, Electrochim. Acta 48 (2002) 407–418.
[15] V.R. Shinde, S.B. Mahadik, T.P. Gujar, C.D. Lokhande, Appl. Surf. Sci. 252 (2006) 7487–7492.
[16] L.-B. Kong, J.-W. Lang, M. Liu, Y.-C. Luo, L. Kang, J. Power Sources 194 (2009) 1194–1201.
[17] C. Lin, J.A. Ritter, B.N. Popov, J. Electrochem. Soc. 145 (1998) 4097–4103.
[18] M. Ramani, B. Haran, R. White, B. Popov, J. Electrochem. Soc. 148 (2001) A374–A380.
[19] V. Panić, T. Vidaković, S. Gojković, A. Dekanski, S. Milonjić, B. Nikolić, Electrochim. Acta 48 (2003) 3805–3813.
[20] M.S. Dandekar, G. Arabale, K. Vijayamohanan, J. Power Sources 141 (2005) 198–203.
[21] Y. Sato, K. Yomogida, T. Nanaumi, K. Kobayakawa, Y. Ohsawa, M. Kawai, Electrochem, Solid State Lett. 3 (2000) 113–116.
[22] C.-C. Hu, W.-C. Chen, K.-H. Chang, J. Electrochem. Soc. 151 (2004) A281–A290.
[23] B.J. Lee, S.R. Sivakkumar, J.M. Ko, J.H. Kim, S.M. Jo, D.Y. Kim, J. Power Sources 168 (2007) 546–552.
[24] J.M. Ko, K.S. Ryu, S. Kim, K.M. Kim, J. Appl. Electrochem. 39 (2009) 1331–1337.
[25] F. Pico, E. Morales, J.A. Fernandez, T.A. Centeno, J. Ibañez, R.M. Rojas, J.M. Amarilla, J.M. Rojo, Electrochim. Acta 54 (2009) 2239–2245.
[26] Z. Algharaibeh, X. Liu, P.G. Pickup, J. Power Sources 187 (2009) 640–643.
[27] J.H. Park, J.M. Ko, O.O. Park, J. Electrochem. Soc. 150 (2003) A864–A867.
[28] C.-C. Hu, C.-C. Wang, Electrochem. Commun. 4 (2002) 554–559.
[29] J.H. Jang, S. Han, T. Hyeon, S.M. Oh, J. Power Sources 123 (2003) 79–85.
[30] G.-J. Lee, S.-I. Pyun, C.-H. Kim, J. Solid State Electrochem. 8 (2004) 110–117.
[31] V.V. Panić, R.M. Stevanović, V.M. Jovanović, A.B. Dekanski, J. Power Sources 181 (2008) 186–192.
[32] P.J. Mahon, G.L. Paul, S.M. Keshishian, A.M. Vassallo, J. Power Sources 91 (2000) 68–76.
[33] V. Panić, A. Dekanski, G. Wang, M. Fedoroff, S. Milonjić, B. Nikolić, J. Colloid Interface Sci. 263 (2003) 68–73.
[34] V.V. Panicǐ, B.Ž. Nikolicǐ, J. Serb. Chem. Soc. 73 (2008) 1083–1112.
[35] P.L. Taberna, P. Simon, J.F. Fauvarque, J. Electrochem. Soc. 150 (2003) A292–A300.
[36] W. Sugimoto, H. Iwata, K. Yokoshima, Y. Murakami, Y. Takasu, J. Phys. Chem. B 109 (2005) 7330–7338.
[37] M. Min, K. Machida, J.H. Jang, K. Naoi, J. Electrochem. Soc. 153 (2006) A334–A338.
[38] J.M. Miller, B. Dunn, Langmuir 15 (1999) 799–806.
[39] M.G. Sullivan, R. Kötz, O. Haas, J. Electrochem. Soc. 147 (2000) 308–317.
[40] A. Braun, J. Kohlbrecher, M. Bärtsch, B. Schnyder, R. Kötz, O. Haas, A. Wokaun, Electrochim. Acta 49 (2004) 1105–1112.
[41] H. Kim, B.N. Popov, J. Power Sources 104 (2002) 52–61.
[42] V.V. Panić, A.B. Dekanski, V.B. Mišković-Stanković, B.Ž. Nikolić, Chem. Biochem. Eng. Q. 23 (2009) 23–30.